A Comparative Evaluation of Optimal Geometric Camera Modelling Options for Airborne and Spaceborne Linear Array Cameras

Azubuike G. Nwosu
Department of Civil Engineering, University of Benin, Benin-city, Nigeria

Raphael Ehigiator-Irughe
Department of Geomatics, University of Benin, Benin-city, Nigeria

Jacob O. Ehiorobo
Department of Civil Engineering, University of Benin, Benin-city, Nigeria

DOI: https://doi.org/10.56293/IJASR.2025.6408

IJASR 2025
VOLUME 8
ISSUE 2 MARCH - APRIL **ISSN: 2581-7876**

Abstract: Multiple variations of the collinearity model have been implemented for spaceborne SPOT and Airborne ASAS imagery. The SPOT model showed better computational stability and achieved sub-pixel misclosures, in some cases at checkpoints. The linear-phi parameter, excluded from some earlier SPOT models, indicated significance and achieved improved performance. A model for airborne ASAS with 15 parameters achieved sub-pixel accuracy at GCPs only. A model utilising higher order polynomials as additional parameters in the airborne model works well but does not render improved performance. INS measurements at 1Hz showed poor results, proving to be inadequate for the imaging frame rate of 40 frames per second. With increasing GCP coverage, misclosures at GCPs (internal accuracy) approach those at ties points (external accuracy).

Keywords: SPOT, ASAS, Camera Model, Linear Array

I. INTRODUCTION

Spaceborne linear array imagery is a major data source for primary data sources for large and medium scale mapping. Airborne linear arrays tend to be employed tactical projects where multi-spectral information is required, or for studies to support spaceborne camera deployments.

Increasingly, data vendors prefer to sell geometrically corrected images (orthophotos), with limited information on the geometric modelling approach used. There are often questions regarding quoted resolution and accuracy of vendor's products that remain unanswered. Processing done for delivered end-products may have serious implications and understanding this is a primary challenge (Sun [1]). Geometric camera modelling linear arrays based on Coupled Charged Devices (CCDs) require a more complex mathematical modelling (Shevlin [2]). This study investigated some approaches to linear array camera model, identifying key issues and parameters, and seeking to develop models that could be applied to a wide range of production lines.

II. THE MODELLING PROBLEM AND OBJECTIVES

Airborne and Spaceborne sensors have dynamics due to camera position and angular attitude changing constantly in ways that are not always systematic. This has been by discussed Mostafa & Hutton [3] Measured support data for position and attitude that are utilised for the modelling system tend to be prone to systematic drifts and need to be properly calibrated or filtered.

This study developed a parametric model for a space-borne linear array sensor (SPOT), and another for an airborne linear array sensor (ASAS). These models were then tested under various combinations of modelling parameters, including the full integration of attitude and positional support data, to seek optimal performance.

III. MATERIALS

The key materials needed are image datasets with accompanied support data orbit ephemeris for satellite imagery, Inertial Navigation System (INS) attitude measurements for both satellite and airborne imagery and GPS/INS positional data.

SPOT satellite data of Aix-en-Provence, France has been used. This is level 1A data with full support data, and only radiometric correction has was applied to it in advance. This image covers a text field of European Organisation for Experimental Photogrammetric Research (OEEPE), appropriately populated with a density of ground control points.

Similarly, airborne ASAS imagery data has been provided by the Biospherics department NASA Goddard Space Flight Centre though a research partnership. All these data sets have full support data. ASAS scenes were available covering an area of Maricopa, Arizona, USA, flown in September 1991 with the older ASAS camera with 29 spectral bands, seven pointing angles, and supported by the 1-5Hz INS system. There are 512 detectors in each linear array imaged from an altitude of about 5000meters, with a footprint/pixel of about 4.25 metres at nadir. The INS data is delivered in merged form at 1 Hz, and sometimes 1 cycle over 2 seconds. Aerial photography of the area was available, taken about the same time as the ASAS coverage. The Maricopa site is fairly flat and reduces the need for a DEM. Image detail are very poor and dominated by striping. GCPs may, therefore, not really be identifiable within 1 pixel accuracy.

Another sets of ASAS data covered the BOREAS (Boreal Ecosystem-Atmosphere Study) sites of Thompson, Manitoba and Prince Albert, Saskatchewan, CANADA, flown in 1994 with the newer ASAS camera with 62 spectral bands, nine pointing angles, and supported by the 30-60Hz INS system. Operated from an altitude of 5000 meters, the nadir image has a footprint/pixel of 3.3 meters across track; at 60 degrees pointing angle this footprint is 6.6 meters. Band 41 was selected for its good image contrast. It had high frequency INS support, but low quality GPS data, and most of the area did not have adequate topographic details for GCPs.

A. SPOT DATA - GEOMETRIC AND RADIOMETRIC ANALYSIS

In 1986, a sun-synchronous, near circular orbiting satellite SPOT1 was launched by France. This polar orbiting satellite carries two CCD-imaging devices (High Resolution Visible HRV1 and HRV2) which operate in panchromatic (P) and multispectral (XS) modes. Each HRV instrument has 3 panchromatic CCD-sensors with 6000 imaging detectors spaced at 13 μm. These CCD-imaging devices are linear arrays operated in pushbroom mode. In panchromatic (PAN) mode, readings from these sensors are integrated into one set of 6000 pixels per line; In multispectral (XS) mode, readings of successive pairs of detectors are added to produce 3 sets of 3000 pixels per line.

Measuring radiation reflected from imaged surfaces at intervals of 1.5004 μsecs (coupled with the spacing of detectors, and the platform altitude) results in an average 10 metres in ground sample distance (GSD) per pixel. The XS mode, samples are at 3.008 micro-seconds with an equivalent GSD of 20 metres. The nominal swath is 60 km (vertical view, see figure 4-1). A mirror attached to the imaging devices allow for viewing angles of up to ±27 degrees, at which the GSD in panchromatic mode could reach 13.5 metres. A stereo made of two views separated by 45 degrees view-angle, possible with a 14-day revisit, would typically give a base-height ratio of 1 (see figure below). The panchromatic band covers 0.51 to 0.73 μm in wavelength, the multispectral bands are 0.5 to 0.59 μm (green), 0.61 to 0.68 μm (red), and 0.79 to 0.89 μm (infrared).

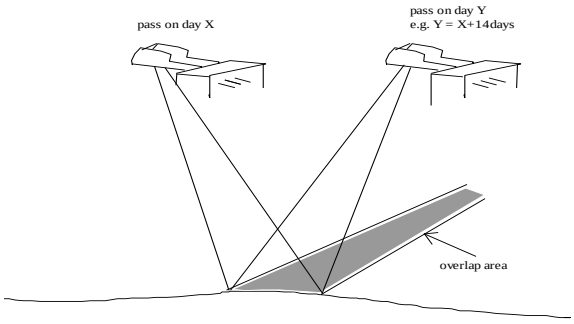

HRV = High Resolution Visible

Figure 1: HRV1 and HRV2 stereoscopic possibilities - From SPOT handbook

Spot scenes are segmented and delivered to cover areas of about 60 km x 60 km; the image is resampled to an average GSD of 10m for the panchromatic image or 20m for the multispectral image. Further pre-processing is done to differentiate the various SPOT products covering both radiometric and geometric corrections as documented in the SPOT imagery user guide (ESA [4]). For camera modelling purposes, the required SPOT product is the Level 1A for which only a radiometric correction has been done.

Though not used in this study, the latest SPOT-6 satellites provide panchromatic images in the range of 1.5m GSD.

B. ASAS GEOMETRIC AND RADIOMETRIC ANALYSIS

ASAS (Irons et al. [5], Nwosu & Muller [6]) is one of NASA's EOS sensors launched in 1998, is an airborne imaging device (single camera) with multi-view capability.

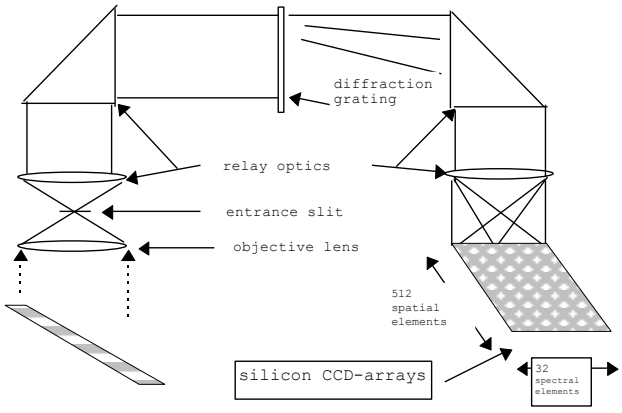

Figure 2: Schematic diagram of the ASAS optics – NASA

The imaging system is a cooled charge-injection-device (CID) with 34 channels in the spectral dimension. 29 of these bands are presently operational at 15 nm bandwidths covering the range 465-871nm. It has 512 pixels in spatial dimension (across flight). Two-dimensional imaging results from aircraft motion programmed to generate between 350 and 500 lines, depending on the flight plan, delivered in a 12-bit digital output.

The effective focal length is determined by the objective lens at 57.2 mm, as far as the geometry of imaging is concerned. This provides a 25-degree FOV, which is about 2.9 minutes per pixel across track, assuming typical C-130 aircraft ground speed (220 knots) and a nominal setting of 48 frames per second. Frame-rate (which determines dwell-time) is programmable for ASAS to values of 3, 6, 12, 24, 48, and 64 frames per second. The optical path is folded by a 90-degree mirror prism in each half to ensure a compact 'U'-shaped optical head. A 75-lines-per-mm

transmission grating, blazed at 530 nm, is located between the two prisms to disperse the radiant energy into its wavelength spectrum, before being directed by the second prism onto the focal plane.

Each CID element has dimensions of 49.6 microns in the across track direction and 81.2 microns in the along track direction. At an altitude of 5000m, this would result in an across-track IFOV of about 4.25m for each CCD element. The stereo imaging mode of ASAS is unique and delivers 7 images of the target-scene at different view-angles with overlap of almost 100 percent. As the aircraft approaches the target area, ASAS takes 7 views from (fore-to-aft) covering the range +45 to -45 at 15-degree steps. The flight plan for ASAS is so rigorously planned that after each imaging view angle, the lens would flick by +15degrees and point approximately at the first line imaged with the previous viewing angle. This cycle continues as the lens moves from one pointing to another.

ASAS data is normally collected in 1 km by 2 km blocks making one 'site pass', with channels 4-32. The first 2 ASAS channels are blocked out and channels 3, 33 and 34 are not operated, resulting in the operational 29 bands as stated earlier. Stewart et al. [7] and Irons et al. [5] have discussed the ASAS imaging system in more detail.

In 1992 the off-nadir tilting platform has been amended to permit up to 75 degrees forward and up to 55 degrees aft (-55, -45, -30, -15, -0, +15, +30, +45, +75 degrees), optionally offering two more off-nadir pointing angles. The new design allows the optical head to rotate for operator-controlled aircraft yaw (kappa) compensation. The old CID array has been replaced a silicon-based, high speed, Thomson CSF Model TH7896A charge-coupled-device (CCD) detector array with 62 spectral bands between 400 and 1000 nm, with a view to improving its performance (Irons et al.., 1992).

The optical system is unchanged, so the effective focal length for the geometry is still 57.2mm. At the focal plane is the 1024 x 1024 CCD array. Each CCD detector measures 19 micrometers in length and width. Every 3 rows of the 186 detector element rows are binned together (in Time delay and Integration - TDI) in the serial readout register resulting in data for 62 spectral bands, achieving 40 frames/second. In the spatial direction, every 2 detector elements are binned into the readout amplifier resulting in 512 pixels perpendicular to the direction of flight. Due to this binning, the effective size of the imaging elements is 38 micrometers across-track; along-track this would be 57 micrometres but a slit, 23 micrometres wide, running along the ASAS optical system allows only this along-track dimension to receive incident energy. The band centres linearly range from 404 nm to 1023 nm at approximately 10 nm intervals and are oriented in the direction of flight. As the platform aircraft flies forward, electronic scanning generates 62 channels of digital image data in the pushbroom fashion that are spatially registered to one another.

The ground sample distance (GSD) is determined by the instantaneous field-of-view (IFOV), the view angle, and aircraft altitude and attitude (mainly pitch). The across-track field-of-view (FOV) is 0.66 mrad/pixel and 0.33 radians (19.3 degrees) across all 512 detectors. At a nadir view angle and an altitude of 5000m above ground level, the full-scene across-track field-of-view is 1.7 km, and the across-track GSD/pixel is 3.3 m. At a 60-degree off-nadir view angle and an altitude of 5000m above ground level, the full-scene across-track field-of-view becomes 3.4 km, and each GSD/pixel 6.6 m. The along-track field-of-view is 0.40 mrad, delivering a footprint of 2 meters for nadir and 8 meters at a view angle of 60 degrees – at 5000 meters altitude.

IV. METHODS

The mathematical setup of the orbit parameter model, derived from a basic collinearity model, will be used to derive the appropriate functional model. This model is programmed and tested with imagery (and support information) from the spaceborne SPOT camera, with various scenarios of GCPs, INS, and additional parameters. Model is then extended additional parameters and tested to determine what parameters are significant and which ones should be dropped (or weighted down) due to their destabilizing effects. These form the basis for a starting point for work on the ASAS airborne camera model.

The mathematical model for ASAS is setup as a standard collinearity system, and a functional model appropriately derived for it. Additional parameters require extensions to the model, and this is also derived separately. The ASAS model is tested for various scenarios of parameters, GCP (and checkpoints) configuration, INS utilisation, and additional parameters. Further evaluations are done after refiltering and re-interpolating INS data to investigate

possibilities for better geometric correction. Evolving methods is experimental with cycles supported by empirical evaluation.

A. SPOT GEOMETRIC AND FUNCTIONAL MODEL

Many SPOT models have been developed in recent years based on precise orbital parameters and other support data (Gugan and Dowman [8], Westin [9]; Radhadevi et. al. [10], Konecny [11], Priebbinow [12] and Kratky [13]). These models are based on the linerar array collinearity model that treats each line of imagery as having the geometry of a perspective image.

Gugan's model was based on a precise orbit with 8 parameters and reported very good results (about 1 pixel). Clerici developed a model similar to Gugan's, but treated the attitude values (integrated from attitude velocities) in slightly different manner. The Konecny model was similar to the classical model for linear arrays and did not involve the processing of orbital parameters. He also had linear rates of change for platform position, and linear and quadratic rates for attitude parameters. The results were not very good. Konecny, with a view to overcoming computational limitations, had an additional parameter model for analytical plotters. The Galguly model was based on Konecny's, but with linear and quadratic rates for both platform position and attitude. RMSE at checkpoints was about 2.5 pixels in planimetry. Westin relied on a simplified orbit which has been discussed in more detail below. Radhadevi et. al. made cosmetic changes to this model by adding more terms but had RMS misclosures at checkpoints of about 3 pixels. Kratky developed one of the earliest models for SPOT but has worked mainly on real time solutions for SPOT in view of the initial limited computational power from standard computer systems.

SPOT Functional model: The adjustment is done in the earth-centred inertial geocentric co-ordinate system (ECI), but transformations are required between these other systems:

- The earth-centred, earth-fixed geocentric system (ECEF)
- A local geodetic system with a known relationship to geographical co-ordinates.
- A sensor co-ordinate system
- A local orbital system which coincides with the attitude reference system when all three attitude values are zero.

Control information in a local co-ordinate system is transformed to geographical co-ordinates, then the ECEF, and finally to the ECI system for use in this model.

$$\mathbf{Xg} = \mathbf{Xs} + \Delta \, Ri \, Rb \, Rs \, \mathbf{x\text{Þ}} \quad (1)$$

where

i. $\mathbf{x\text{Þ}}$ = image co-ordinates vector
ii. Xg = ground co-ordinates vector in ECI
iii. Xs = satellite position vector in ECI
iv. Δ = scale factor
v. Ri = Rotation from the orbital reference system to the ECI
vi. Rb = Rotation between the attitude reference system and the orbital system.
vii. Rs = Rotation between the sensor and the attitude reference system; the primary rotation in omega is the mirror inclination; it would also take care of the CCD-sensor off-sets, if any. Rs is optional because the system can accommodate for the absence of this rotation in the model. Accordingly, the mirror inclination angle can be used as an initial value for omega in Rb instead of a zero value.

The reverse equation is:

$$\mathbf{x\text{Þ}} = 1/\Delta \, . \, R \, . \, \mathbf{(Xg - Xs)} \quad (2)$$

where $R = (Rs \, . \, Rb \, . \, Ri)$

In matrix form, this becomes:

$$\begin{bmatrix} 0 \\ y_p \\ -c \end{bmatrix} = \frac{1}{\Delta}\begin{bmatrix} r_{11} & r_{12} & r_{13} \\ r_{21} & r_{22} & r_{23} \\ r_{31} & r_{32} & r_{33} \end{bmatrix} \bullet \begin{bmatrix} Xg - Xs \\ Yg - Ys \\ Zg - Zs \end{bmatrix} \quad (3)$$

y_p is the y-image co-ordinate, and c is the focal length of the camera.

The SPOT header file provides a scene-centre-time from which imaging times for any lines could be calculated using the CCD integration time which is 1.5004 μs for SPOT. Radial data from the ephemeris data is fitted to a third-degree polynomial with respect to time. Ephemeris data is also used to calculate the time at the ascending node, enabling the dynamic calculation of the travel angle at any image point. The radius at any image point could be used to generate the camera position co-ordinates by the inverse transformation with the orthogonal matrix of Keplerian rotation angles (Ri); see below. Of the Keplerian rotations parameters, Right ascension (Ω) and Inclination (I) remain fairly constant; only the travel angle (ν) is changing rapidly with time.

$$F_1 = 0 = -c \bullet \frac{r_{11}(Xg - Xs) + r_{12}(Yg - Ys) + r_{13}(Zg - Zs)}{r_{31}(Xg - Xs) + r_{32}(Yg - Ys) + r_{33}(Zg - Zs)} \quad (4)$$

$$F_2 = y_p = -c \bullet \frac{r_{21}(Xg - Xs) + r_{22}(Yg - Ys) + r_{33}(Zg - Zs)}{r_{31}(Xg - Xs) + r_{32}(Yg - Ys) + r_{33}(Zg - Zs)} \quad (5)$$

The adjustment could correct five observations y-image co-ordinate, time of imaging Ground Control Points (GCP) (t, equivalent to x-pixel co-ordinate), Longitude (**φ**), Latitude (**λ**) and height (**h**).

[yp, t, φ, λ, h].

The 8 parameters of orientation to be corrected are:

[I_o, Ω_o, t_o, r_o, ω_o, ρ_o, κ_o, ρt_o].

ρto is the linear component of the phi rotational parameter. The others are Inclination (I), Right Ascension (Ω), Time at Ascending node (t_o), Orbital radius at Ascending node (r o). the central travel angle is derived by equation (2 and 3).

A Taylor's series expansion of the collinearity equations is done but only the first order terms are taken.

$$A_k = \begin{bmatrix} \frac{\delta F_1}{\delta y_p} & \frac{\delta F_1}{\delta t} & \frac{\delta F_1}{\delta \varphi} & \frac{\delta F_1}{\delta \lambda} & \frac{\delta F_1}{\delta h} \\ \frac{\delta F_2}{\delta y_p} & \frac{\delta F_2}{\delta t} & \frac{\delta F_2}{\delta \varphi} & \frac{\delta F_2}{\delta \lambda} & \frac{\delta F_2}{\delta h} \end{bmatrix} \quad (6)$$

$$B_k = \begin{bmatrix} \frac{\delta F_1}{\delta I} & \frac{\delta F_1}{\delta \Omega} & \frac{\delta F_1}{\delta t_o} & \frac{\delta F_1}{\delta r_0} & \frac{\delta F_1}{\delta w_o} & \frac{\delta F_1}{\delta \rho_0} & \frac{\delta F_1}{\delta \kappa_0} \\ \frac{\delta F_2}{\delta I} & \frac{\delta F_2}{\delta \Omega} & \frac{\delta F_2}{\delta t_o} & \frac{\delta F_2}{\delta r_0} & \frac{\delta F_2}{\delta w_o} & \frac{\delta F_2}{\delta \rho_0} & \frac{\delta F_2}{\delta \kappa_0} \end{bmatrix} \quad (7)$$

The condition equation can be written as:

$$Av + B\xi = f \quad (8)$$

where v is the vector of measurement residuals, ξ are the corrections to parameters which are initially given as approximate values. Formulated in this way, the equation could be singular in a poor GCP configuration (Gugan [7], Westin [8]), mainly due to the high correlation between parameters (mainly phi and platform motion). It could be stabilised by padding with 'fictitious' equations, taking this shape:

$$\begin{bmatrix} A & 0 \\ 0 & I \end{bmatrix} \begin{bmatrix} v \\ v_p \end{bmatrix} + \begin{bmatrix} B \\ -I \end{bmatrix} \xi = \begin{bmatrix} c \\ 0 \end{bmatrix} \quad (9)$$

Simply, unknowns could be treated as fictitious observations with associated weights. These weights are usually set from experience and fine-tuned by trial and error. Using weights to effect the stability articulated above, the solution by Mikhail [14] is:

if **Q** is the apriori cofactor matrix for the measurements
and $\mathbf{W}_{pp}$ is the apriori weight matrix for the parameter estimates.
then

(10)

v can always be calculated after a convergence has been achieved from a few iterations.

$$v = A^T (AQA^T)^{-1} (f - B\xi) \quad (11)$$

Attitude and positional parameters of linear-array imaging are known to be substantially correlated.

Omega (roll) proved to be the main parameter to be solved. Two GCPs, one on each side usually offered a very stable equation system; with one GCP in the upper section and one in the lower section, a very unstable system tends to emerge.

A single image bundle resection is done initially. If tie points are needed for a good relative orientation, they could be measured after this computation. This initial orientation assures that reliable approximate values for these tie points are calculated. After tie points are measured, a two-step adjustment is done, initially a single image bundle adjustment of each of the two images, and finally with a block adjustment of both images together.

This SPOT model converges in 3 or 4 iterations; beyond 5 iterations is usually a sign of a poor GCP configuration, or deficient modelling.

B. ASAS GEOMETRIC AND FUNCTIONAL MODEL

ASAS is imaged from an airborne platform prone to perturbations that are far more random than systematic due to aircraft vibrations and air turbulence. The attitude changes of the imaging platform can be measured with INS gyros. These INS-parameters will vary between systems, but a generic approach will take care of these possibilities, including when there is no support data. Three test models cover three possibilities:

- when there is no support data but GCPs are available.
- when positional data and GCPs are available (no attitude data).
- when both positional and attitude data are available; GCPs are also used for refinement.

The third model is the nearest realisation to an optimum model, but performance would depend on the frequency and precision of INS data collection, and the method of collection and merging.

The strategy is to employ all support information that is available, but to refine these data with GCPs. In all three cases the linear array collinearity model is used, treating each line of imagery as having a perspective geometry.

Collecting and merging INS-information, and importing it into a camera model can be critical and raises many questions. Two INS systems were available for assessment, one makes measurements at 1Hz, and the other at 30-60Hz.

ASAS Functional model: The equation linking the image co-ordinates to the ground co-ordinates of a GCP is given by the direct collinearity equation as utilised for the SPOT system above.

Camera position as well as camera attitude angles and modelled with 2nd degree polynomials. *xp* is used in place of elapsed time.

$$X_s = X_{s0} + X_{s1} . x_p + X_{s2} . x_p . x_p \quad (12)$$

$$Y_s = Y_{s0} + Y_{s1} . x_p + Y_{s2} . x_p . x_p \quad (13)$$

$$Z_s = Z_{s0} + Z_{s1} . x_p + Z_{s2} . x_p . x_p \quad (14)$$

R = f (kappa, phi, omega)

$$\text{kappa} = \kappa + \kappa_1 . x_p + \kappa_2 . x_p . x_p \quad (15)$$

$$\text{phi} = \varphi + \varphi_1 . x_p + \varphi_2 . x_p . x_p \quad (16)$$

$$\text{omega} = \omega + \omega_1 . x_p + \omega_2 . x_p . x_p \quad (17)$$

x_p = line-number * CID-element-size-in-y / 2

Here, element size-in-y is used instead of x, and scaled down for stability.

y_p is the y-image co-ordinate, and c is the focal length of the ASAS camera.

$$R = \begin{bmatrix} \cos k & \sin k & 0 \\ -\sin k & \cos k & 0 \\ 0 & 0 & 1 \end{bmatrix} \bullet \begin{bmatrix} \cos\varphi & 0 & \sin\varphi \\ 0 & 1 & 0 \\ -\sin\varphi & 0 & \cos\varphi \end{bmatrix} \bullet \begin{bmatrix} 1 & 0 & 0 \\ 0 & \cos\omega & \sin\omega \\ 0 & -\sin\omega & \cos\omega \end{bmatrix} \quad (18)$$

Since they would not be error free, the adjustment could compute corrections (residuals) for the five observations x-image, y-image co-ordinate, Eastings (E), Northings (N) and Height (h). $[x_p, y_p, E, N, h]$

The benefit is to monitor these observations for gross errors, but these residuals are usually computed later.

The 15 parameters include linear and polynomial parameters of orientation to be corrected. Phi is fixed to the value of the pointing angle and, with its linear and polynomial components dropped from the model, leaving:

$$[\kappa_0, \omega_0, \kappa_1, \omega_1, \kappa_2, \omega_2, X_0, Y_0, Z_0, X_1, Y_1, Z_1, X_2, Y_2, Z_2] \quad (19)$$

A Taylor's series expansion of the collinearity equations is done but only the first order terms are used. The matrix takes this form in equation (19) and (20).

$$A_k = \begin{bmatrix} \frac{\delta F_1}{\delta \kappa_0} & \frac{\delta F_1}{\delta \omega_0} & \frac{\delta F_1}{\delta \kappa_1} & \frac{\delta F_1}{\delta \omega_1} & \frac{\delta F_1}{\delta \kappa_2} & \frac{\delta F_1}{\delta \omega_2} & \frac{\delta F_1}{\delta X_0} & \frac{\delta F_1}{\delta Y_0} & \frac{\delta F_1}{\delta Z_0} \cdots \\ \frac{\delta F_2}{\delta \kappa_0} & \frac{\delta F_2}{\delta \omega_0} & \frac{\delta F_2}{\delta \kappa_1} & \frac{\delta F_2}{\delta \omega_1} & \frac{\delta F_2}{\delta \kappa_2} & \frac{\delta F_2}{\delta \omega_2} & \frac{\delta F_2}{\delta X_0} & \frac{\delta F_2}{\delta Y_0} & \frac{\delta F_2}{\delta Z_0} \cdots \end{bmatrix} \quad (20)$$

$$B_k = \begin{bmatrix} \frac{\delta F_1}{\delta y_p} & \frac{\delta F_1}{\delta x_p} & \frac{\delta F_1}{\delta E} & \frac{\delta F_1}{\delta N} & \frac{\delta F_1}{\delta H} \\ \frac{\delta F_2}{\delta y_p} & \frac{\delta F_2}{\delta x_p} & \frac{\delta F_2}{\delta E} & \frac{\delta F_2}{\delta N} & \frac{\delta F_2}{\delta H} \end{bmatrix} \quad (21)$$

Where n is the number of GCPs. The condition equation can be written as:

$$Av + B\xi = f \quad (22)$$

These equations could be singular without enough GCPs, mainly due to the high correlation between parameters. It could be stabilised with similar measures as done with the SPOT model.

Similarly, the solution by Mikhail (1976) is as executed similar to the one for SPOT. Necessary changes are made to the model to implement and compute that various modelling options for investigation.

V. RESULTS OF TEST OF SPOT SPACEBORNE CAMERA MODELS

A. EXPERIMENT 1: ORBIT PARAMETER MODEL TESTED ON SPOT - 8 PARAMETERS

This is a refinement of the Westin model with orbital parameters reduced to four for simplicity and efficiency and computed in the Earth Centred Inertial Geocentric Co-ordinate System (ECI). We found the linear phi parameter to be significant, contrary to the approach of Westin (1990), and that it improves the modelling results.

Experiment 1 Scenario 1 Spot Orbit model with linear phi

Added refinements is the addition of a linear-phi parameter which was found to be significant during simulations and resulted in improved performance with a total of 8 parameters.

Table 1: Experiment 1 scenario 1 SPOT Orbit model with linear phi

No of GCPs	No of Chkpts	RMSE GCPs (pix)	RMSE Chk Pts (pix)
18	0	0.97	nil
14	4	0.89	1.3
10	8	0.75	1.25
7	11	0.51	1.40

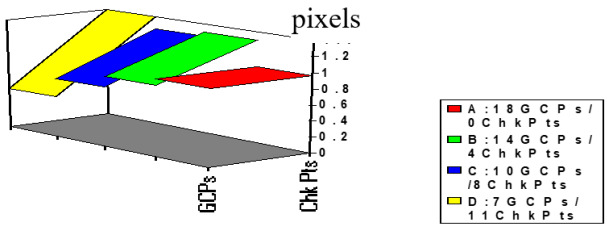

Figure 3: Experiment 1 scenario 1 SPOT Orbit model with linear phi

Experiment 1 Scenario 2 Spot Orbit model on ties points

This model is similar to the one above. Two computations were done, one with ties points and the other without utilise tie points. It shows a general conformist trend of having higher residuals at checkpoints than at GCPs used in computing orientation. With fewer controls you have a better fit at GCPs but tend to have higher residuals at checkpoints – internal accuracy versus external accuracy. It showed slightly better results with tie points than without tie points.

Table 2: Experiment 1 scenario 2 SPOT Orbit model with ties points

No of GCPs	No of chkpts	RMSE GCPs (pixels) 1-with tie pts 2-No tie pts	RMSE chkPts (pixels) 1-tie pts 2-No tie pts
17	0	0.92 0.92	nil
13	4	0.90 0.86	0.99 1.01
11	6	0.83 0.92	1.27 0.85
9	8	0.80 0.75	1.36 0.89
7	10	0.78 0.73	1.25 1.35

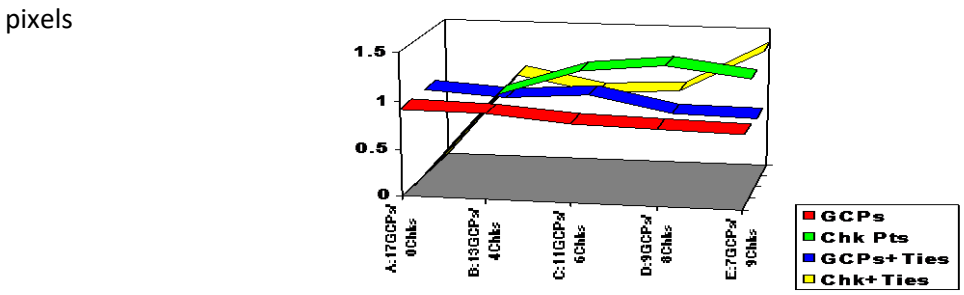

Figure 4: Experiment 1 scenario 2 SPOT Orbit model with ties points

Experiment 1 Scenario 3 Spot Orbit model many GCPs

This is the same as case study 3 but computed on a different SPOT image. No tie points are employed in a single bundle resection.

Table 3: Experiment 1 scenario 3 SPOT Orbit model many GCPs

No of GCPs	No of Chkpts	RMSE GCPs (pix)	RMSE ChkPts (pix)
26	0	0.89	nil
15	11	0.70	1.2
9	17	0.62	1.2
7	19	0.45	1.3

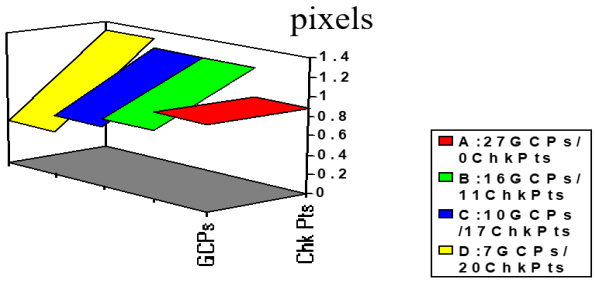

Figure 5: Experiment 1 scenario 3 SPOT Orbit model many GCPs

The behaviour here shows that with an adequate number and distribution of GCPs, the residuals at GCPs approach the value of residuals at checkpoints. But with fewer controls you seem to have a better fit at GCPs.

Experiment 1 Scenario 4 merging ECEF and ECI

Some generic facilities were introduced to seek wider application of the model to both airborne and space-borne systems, resulting in a further simplified model. The solution is still orbital, but it is assumed that during the period of imaging a spot scene, the ECEF and ECI system coincide, so there is no need to transform to-and-from the orbital system. The parameters remain the same for a total of 8. Computations were slightly faster here because of the absence of inertial transformations. This shows a slight improvement on the full Orbit model, despite using a less complex algorithm with less computational load.

Table 4: Experiment 1 scenario 4 merging ECEF and ECI

No of GCPs	No of chkpts	RMSE GCPs (pix) with tie pts without tie pts	RMSE chk. Pts (pix)
17	0	0.92 0.92	nil
13	4	0.90 0.86	0.99 1.01
11	6	0.83 0.92	1.27 0.85
9	8	0.80 0.75	1.36 0.89
7	10	0.78 0.73	1.25 1.35

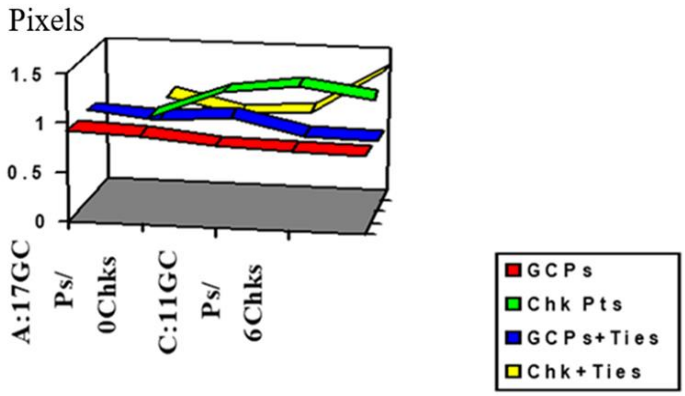

Figure 6: Experiment 1 scenario 4 merging ECEF and ECI

B. EXPERIMENT 2: AN EXTENDED MODEL TESTED ON SPOT

This is similarly simplified Orbit model computed in the ECEF co-ordinate system, but with more parameters.

Experiment 2 Scenario 5 with extended parameters

Parameters are added to a total of 13, with linear and second-degree parameters for kappa, phi and omega attitude parameters.

Table 5: Experiment 2 scenario 5 with extended parameters

No of GCPs	No of chkpts	RMSE GCPs (pix) with tie points without tie pts	RMSE chk. Pts (pix) with tie points without tie pts
17	0	0.75 0.75	nil
13	4	0.61 0.47	1.09 1.79
11	6	0.64 0.44	0.87 1.45
9	8	0.47 0.36	1.36 1.44
7	10	0.29	1.35

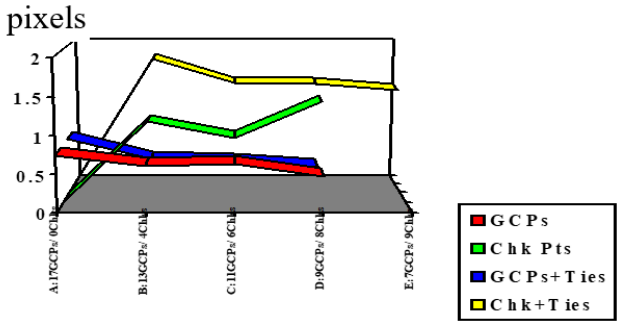

Figure 7: Experiment 2 scenario 5 with extended parameters

This model shows better fitting to GCPs than, but it shows more residuals at checkpoints. Increasing the number of parameters would not always give improved results, in fact it could give poorer results if the maximum number needed are exceeded. Essentially, some parameters are insignificant.

C. EXPERIMENT 3: USING NAVIGATIONAL DATA TO RUN AIRBORNE MODEL ON SPOT

SPOT imagery is supplied with a predicted ephemeris. Combined with the attitude information, these are equivalent to the output of a typical INS system.

Experiment 3 scenario 6: using only navigational data to model SPOT

A slightly different model was developed that relied on navigational information (SPOT ephemeris), without adjustment in the model. This is with a view to seeking general applicability to both space-borne and airborne imagery. This assumes that navigational information is good and reliable. This did not deliver good results, suggesting that SPOT navigational data cannot be relied on solely in a good camera model.

Table 6: Experiment 3 scenario 6 model with only navigational data

No of GCPs	No of chkpts	RMSE GCPs (pix) with tie points without tie pts	RMSE chk. Pts (pix)
17	0	2.09 2.09	nil
13	4	2.16 1.61	2.13 1.80

11	6	2.3 1.6	2.16 2.08
9	8	2.32 1.80	2.32 1.80
7	10	2.37 1.87	2.37 2.01

D. SPOT TESTS DISCUSSION

The linear phi parameter is significant and improves results. The models show a general conformist trend of having higher residuals at checkpoints than at GCPs used in computing orientation. With fewer controls you have a better fit at GCPs - internal accuracy - but tend to have higher residuals at checkpoints - external accuracy. It showed slightly better results with tie points than without tie points. With adequate number, and distribution, of GCPs, the residuals at GCPs approach the value of residuals at checkpoints. Merging the ECEF and ECI systems into one angular set of rotations in a simplified model produced slightly better results. Increasing the number of parameters would not always give improved results; in fact, it could give poorer results if some of the parameters are insignificant. Employing navigational data of poor quality is not very useful.

V. RESULTS OF TEST OF THE ASAS AIRBORNE CAMERA MODELS

Selected points on ASAS imagery were identified on the aerial photographs and their ground co-ordinates recorded on the analytical plotter. It is assumed, considering that ASAS imagery is dominated by striping, that there is an identification error of 1 pixel, in this case about 5 meters. When the RMS misclosures stated in the above paragraph are taken into consideration, we assume that the GCPs have a RMSE of 8 metres due to error propagation.

Three Models have been developed and tested in this project:

- a collinearity model for airborne linear array imagery (with ASAS) computed with GCPs but without INS support data.
- a collinearity model for airborne linear array imagery (ASAS) computed with GCPs but with limited INS support data (camera position only).
- a collinearity model for airborne linear array imagery (ASAS) with full INS support data at 1Hz, relying heavily on GCPs in the model. This also offers the option of additional parameters.
- The model in No 3. has also been tested with ASAS with full INS attitude data at 70 Hz and GPS navigational data, with GCPs used for refinement. These tests were mainly for evaluation of attitude data at various frequencies of measurement.

In all cases the low quality of the GCPs must have degraded results. Other degradation components are from identification of GCPs in the image and their extraction from maps, which would be at least one pixel.

A. EXPEIMENT-1: COLLINEARITY MODEL WITH ONLY GCPS ON ASAS

This is based on the collinearity model for airborne linear arrays. It does not use navigational data; it is based on attitude parameters and position of the imaging platform, but phi is dropped as a parameter, and consequently its linear and second-degree terms, resulting in a total of 15 parameters.

Experiment 1 scenario 1 on ASAS with only GCPs

With 15 parameters and only 10 GCPs, it was not possible to isolate some points to use as checkpoints. The model converged very well in a few iterations, rendering sub-pixel accuracy, confirming the possibility of modelling the effects of linearly changing camera positions. Test results further showed that deviations away from GCPs was up to four times as recorded at GCPs. This model may not adequately handle across-track displacements due to attitude changes and relief.

Table 7: Experiment 1 scenario 1 on ASAS with GCPs

View No	Imaging angles	RMSE -X pix	RMSE -Y pix	RMSE-XY pix
1	45.0	1.685	0.429	1.057
2	29.5	1.091	0.532	0.812
4	0.0	1.160	0.709	0.939

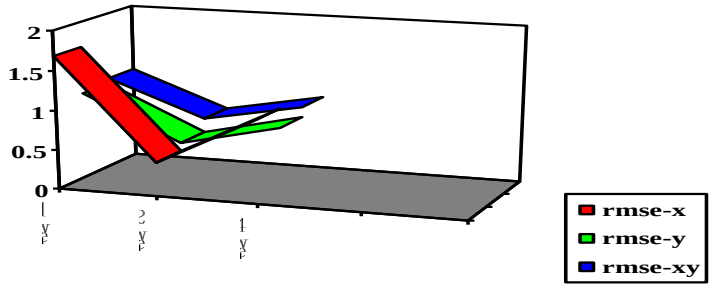

Figure 8: Experiment 1 scenario 1 on ASAS with only GCPs

The geometric quality of an ASAS view may not be predictable because a lot depends on platform stability during the flight, and this determines the quality of resection. With similar platform turbulence, views nearer the vertical are better; but in this case view 2 has outperformed view 4.

B. EXPERIMENT 2: AIRBORNE MODEL TESTED ON ASAS WITH GCPS AND INS

This is also the collinearity model like the previous case, but it is assumed that INS positional data is of suitable accuracy to model platform position accurately. Here we are solving for only the three attitude parameters and their three linear and second degree coefficients, making a total of 9 parameters.

Experiment 2 scenario 2 on ASAS with INS

Assuming good INS position data, and solving for 9 parameters of attitude. GCPs are check points. Only the nadir view (number 4) converged, indicating that the positional data is not of sufficient accuracy and6 may be prone to second-degree drifts.

Table 8: Experiment 2 scenario 2 on ASAS with only INS

View No	Imaging angle deg	RMSE -X pix	RMSE -Y pix	RMSE -XY pix
4	0.0	1.261	2.472	1.867

Note that the mis-closures shown are only for GCPs. Checkpoints showed substantial differences in Y-pixel (up to 4 times as much).

Experiment 2 scenario 3 on ASAS with GCPs and INS

Full INS support is just for orientation but GCPs are used for refinement (or calibration). 9 parameters are corrected, 3 for attitude and 6 for platform position because of the presence of drift errors in the later.

The GCP field seemed to be weak, with some showing high residuals. There were much higher residuals in X-flight direction than in Y- due to the method of computation and because INS measurements are modelled with image line-numbers; time synchronisation errors will normally show up in X.

Table 9: Experiment 2 scenario 3 on ASAS with INS and GCPs - collinearity model

view No	imaging angle deg	RMSE-X pixel	RMSE-Y pixel	RMSE-XY pixel
2s	30	5.25	2.01	3.63
4	0	2.19	0.72	1.46

The orientation relies solely on INS data but GPPs are used for refinement (calibration). When corrected for the precision of GCPs and point identification on the ASAS images, these residuals would be lower, but results show that the 1Hz INS used here is not adequate.

Experiment 2 scenario 4 on ASAS with INS, GCPs and time sync

Same model as above, but some attempt is made to synchronise the INS time with that of imaging by shifting the measurements. These results are limited because the INS frequency is too low at 1 Hz.

Table 10: Experiment 2 scenario 4 - ASAS with GCP and INS time sync

View No	RMES-XY pix with no timing shift in INS	RMES-XY pix with 1sec shift of in INS	RMES-XY pix with -1sec shift in INS	RMES-XY pix with -2sec shift in INS
2	3.63	not con-verged	3.65	not converged
4	1.46	1.40	1.60	1.78

This shows that with low frequency INS, time synchronisation would not improve results.

C. EXPERIMENT 3: AIRBORNE MODEL TESTED ON ASAS WITH ADDITIONAL PARAMETERS

The same collinearity model with full INS support, and GCPs. Same 9 parameters are corrected, 3 for attitude and 6 for platform position, but it is now extended with additional parameters.

Experiment 3 scenario 5 with additional parameters.

Table 11: Experiment 3 scenario 5 ASAS with additional parameters

View No	Imaging angle deg	with additionl params RMSE -X pix	with additionl params RMSE -Y pix	with additionl params RMSE -XY pix
2	30	5.03	1.73	3.38
4	0	1.80	0.74	1.27

Experiment 3 scenario 6 with additional parameters and time sync

Synchronising the INS time with that of imaging by shifting the measurements we have:

Table 12: Experiment 3 scenario 6 ASAS with additional parameters and time sync

View Number	RMES-XY pix with no timing correction in INS	RMES-XY pix with correction of 1 second in INS	RMES-XY pix with correction of -1 second in INS	RMES-XY pix with correction of --2 seconds in INS
2	3.38	not converged	3.56	5.8
4	1.27	1.24	1.43	1.92

This shows that with low frequency INS, time synchronisation would not improve results.

INS data needs to be properly synchronised with image data. This problem is caused by drifts in the two clocks used for the different systems. View 4 results seemed to be fairly in order. The other views require better synchronisation to match these results, but this has been limited by the frequency of INS (1 Hz), and the INS data in provided in merged form. The higher degree of over-sampling at higher off-nadir view-angles leads to higher identification errors of GCPs (due to much larger footprint) and this would further deteriorate the orientation of these views. This model relies highly on the INS measurements, and where they are of inadequate quality the equation system deteriorates rapidly. The stability of the nadir view confirms success in developing the geometric model estimation under varying camera positional dynamics (pointing angle, rotation, and shaking) using higher order polynomial equations in airborne imaging systems.

D. ASAS TESTS DISCUSSION

With a good distribution of GCPs, nadir view misclosures are sub-pixel at the GCPs. Tests with only GCPs, modelling attitude parameters (without phi), and the position of the imaging platform, showed that deviations away from GCPs could be up to four times as recorded at GCPs. These models may not adequately handle across-track displacements due to attitude changes and relief.

Generally, platform instability has a disproportionate effect on off nadir camera views, resulting in poor resection and convergence. Using 5Hz INS data as accurate is shown to distort the model with the camera frame rate at 40Hz. As INS measurements are modelled with image line-numbers, time synchronisation errors show up in X, resulting in much higher residuals in X-flight direction than in Y. Trying to synchronise low frequency INS data is not helpful.

Extending the ASAS airborne collinearity model with additional parameters gives decent results, but combined with poor INS data would not lead to improved results. INS data synchronisation becomes necessary when two different clocks are used for the INS and Imaging systems, with attendant drifts. Off-nadir view-angles have higher identification errors for GCPs (due to much larger footprint and smear), and this further deteriorates the modelling of these views.

None of the tests reported on airborne linear array orientation yielded sub-pixel residuals on checkpoints. This is mainly due to the limitations in data quality for INS and GPS. Tests done independently with the high-quality INS-GPS data (Hutton and Lithopoulos [15]) show that sub-pixel accuracy is now possible. The important thing here, as well as shown with the Stuttgart model Fritsch (1997), is that INS-GPS could be calibrated within a block adjustment. With directly measured camera orientation, this technique could still be used, especially in those cases where INS-GPS have unusual drifts and repeating data collection would be too expensive.

VI. CONCLUSION

The SPOT spaceborne model shows a general conformist trend of having higher residuals at checkpoints than at GCPs used in computing orientation. With fewer controls you have a better fit at GCPs - internal accuracy but tend to have higher residuals at checkpoints – external accuracy. It showed slightly better results with tie points than

without tie points. With adequate number, and distribution, of GCPs, the residuals at GCPs approach the value of residuals at checkpoints.

Merging the ECEF and ECI systems into one angular set of rotations in a simplified model produced slightly better results. Increasing the number of parameters would not always give improved results; in fact, it could give poorer results if some of the parameters are insignificant. Employing navigational data of poor quality is not very useful.

The airborne ASAS collinearity model with only GCPs, modelling attitude parameters (without phi) and the position of the imaging platform, showed that deviations away from GCPs was up to four times as recorded at GCPs. This model may not adequately handle across-track displacements due to attitude changes and relief.

Generally, platform instability has a disproportionate effect on off nadir camera views, resulting in poor resection and convergence. Using 5Hz INS data as accurate is shown to distort the model where the camera frame rate is 40Hz. As INS measurements are modelled with image line-numbers, time synchronisation errors show up in X, resulting in much higher residuals in X-flight direction than in Y. Trying to synchronise low frequency INS data is not helpful. Extending the ASAS airborne collinearity model with additional parameters gives decent results, but combined with poor INS data would not lead to improved results.

INS data synchronisation becomes necessary when two different clocks are used for the INS and Imaging systems, with attendant drifts. Off-nadir view-angles have higher identification errors for GCPs (due to much larger footprint and smear), and this further deteriorates the modelling of these views. None of the tests reported on airborne linear array orientation yielded sub-pixel residuals on checkpoints. This is mainly due to the limitations in data quality for INS and GPS. Tests done independently with the high quality INS-GPS data (Hutton and Lithopoulos [15]) already show that sub-pixel accuracy is now possible.

The important thing here, is that INS-GPS could be calibrated within a block adjustment. With directly measured camera orientation, this technique could still be used, especially in those cases where INS-GPS have unusual drifts and repeating data collection would be too expensive.

Acknowledgements

Bill Kovalick and Phil Dabney, NASA GSFC

Prof. J-P Muller, UCL Mulllard Space Science Laboratory

References

1. Sun, Y. (2024), "Geometric calibration of the linear-array whiskbroom optical satellites based on look-angle corrections", Journal of Physics Conference Series 2724(1):012032.
2. Shevlin, F. (1994), "Kinematic Modelling of Scanner Trajectories", Spie proceedings on Image and Signal Processing
3. Mostafa, M. & Hutton, J. (2001), "Airborne Remote Sensing Without Ground Control", Proceedings. IEEE 2001 International Geoscience and Remote Sensing Symposium (Cat. No.01CH37217) 9-13 July 2001.
4. ESA (2016) https://earth.esa.int/eogateway/ documents/20142/37627/SPOT-6-7-imagery-user-guide.pdf
5. Irons, J.R., Ronson, K., Williams, D. L., Irish, R.R., & Huegel, F.G. (1991), "An Off- Nadir-Pointing Imaging Spectroradiometer For Terrestrial Ecosystem Studies", IEEE Trans Vol. 29 No.1, 1991, pp. 66-74.
6. Nwosu, A.G., & Muller, J-P. (1992), "Technical specifications for a Camera Model for the NASA-Advanced Solid-State Array Spectroradiometer (ASAS)", Proceedings of ASPRS/ ACSM Convention, Monitoring and Mapping Global Change, Washington D.C. 3-7 August, pp. 364-373, 1992.
7. Stewart, S. E., Buntzen, R. R., & Carbone, J. (1985), "Advanced CID Array Multispectral Pushbroom Scanner", Laser Focus / Electro Optics, Vol. 21, No. 6, 1985, pp. 88-100.
8. Gugan, D. J., & Dowman, I.J. (1988), "Topographic Mapping from SPOT Imagery", Photogrammetric Engineering and Remote Sensing, Vol. 54, No. 10, October 1988, pp. 1409-1414.
9. Westin, T. (1990), "Precision Rectification of SPOT Imagery", PE&RS, Vol. 56, No. 2, pp. 247-253.

10. Radhadevi, P.V., Sasikumar, T.P., & Ramachandran, R. (1994), "Orbit Attitude Modelling and Derivation of Ground Co-ordinates from SPOT Stereopairs", ISPRS Journal of Photogrammetry and Remote Sensing, 49(4): pp 22-28.
11. Konecny, G. (1987), "Geometric Evaluation of SPOT Imagery. CERCO seminar on the SPOT system and its applications", Paris, September 6-9, 1988, pp. 20-53.
12. Priebbenow, R & Clerici, E (1988). Cartographic Applications of SPOT. Imagery. Proceedings of ISPRS Congress, Commission IV, 1988.
13. Kratky, V. (1989), "Rigorous Stereo-photogrammetric Treatment of SPOT Images', PE&RS, vol. 55, No. 3, pp. 311-316, March 1989.
14. Mikhail, E.M. - with contributions from Ackermann F. (1976), "Observations and Least Squares", New York: EIP; xi, 497 pages.
15. Hutton, J. J., & Lithopoulos, E. (1980), "Airborne Photogrammetry Using Direct Camera Orientation Measurements", Geoinformation 6/1998, S. 363-370.